RSC Advances

PAPER

View Article Online
View Journal | View Issue

Cite this: *RSC Adv.*, 2023, **13**, 3234

Durable composites by vulcanization of oleyl-esterified lignin†

Menisha S. Karunarathna,[a] Charini P. Maladeniya,[a] Moira K. Lauer,[a] Andrew G. Tennyson *[ab] and Rhett C. Smith *[a]

Productive utilization of lignocellulosic biomass is critical to the continued advancement of human civilization. Whereas the cellulose component can be efficiently upconverted to automotive fuel-grade ethanol, the lack of upconversion methods for the lignin component constitutes one of the grand challenges facing science. Lignin is an attractive feedstock for structural applications, in which its highly-crosslinked architecture can endow composite structures with high strengths. Prior work suggests that high-strength composites can be prepared by the reaction of olefin-modified lignin with sulfur. Those studies were limited to ≤5 wt% lignin, due to phase-separation of hydrophilic lignin from hydrophobic sulfur matrices. Herein we report a protocol to increase lignin hydrophobicity and thus its incorporation into sulfur-rich materials. This improvement is affected by esterifying lignin with oleic acid prior to its reaction with sulfur. This approach allowed preparation of esterified lignin–sulfur (ELS) composites comprising up to 20 wt% lignin. Two reaction temperatures were employed such that the reaction of ELS with sulfur at 180 °C would only produce S–C bonds at olefinic sites, whereas the reaction at 230 °C would produce C–S bonds at both olefin and aryl sites. Mechanistic analyses and microstructural characterization elucidated two ELS composites having compressive strength values (>20 MPa), exceeding the values observed with ordinary Portland cements. Consequently, this new method represents a way to improve lignin utilization to produce durable composites that represent sustainable alternatives to Portland cements.

Received 7th November 2022
Accepted 11th January 2023

DOI: 10.1039/d2ra07082k

rsc.li/rsc-advances

Introduction

Agricultural processes generate gigaton quantities of lignocellulosic biomass each year.[1,2] Given that biomass contains an enormous amount of CO_2 captured and removed from the atmosphere, this biomass represents a priceless contribution to sustainability, but it is significantly underutilized as a material in its own right. For example, structural materials produced from lignocellulosic biomass would be carbon-negative alternatives to the petrochemically-derived materials widely used in residential and commercial applications. Although significant progress has been made in the upconversion of cellulosic biomass to ethanol, a fuel critical to the green economy, the residual lignin produced after cellulose extraction is largely discarded as waste or burned as a low-efficiency fuel.[3–5]

Recent work by our group, however, revealed that lignin–sulfur composites exhibit mechanical strengths rivalling those of many commercially-available structural materials.[6–9] A limitation of these composites is that in some applications the lignin component was capped at 5 wt%, even if the monomer feed contained 20 wt% of the lignin derivative. This upper limit of 5 wt% lignin can be attributed to the low miscibility of hydrophilic lignin with hydrophobic sulfur. We therefore hypothesized that esterifying lignin hydroxyl moieties, which are hydrophilic, with unsaturated fatty acid chains, which are hydrophobic, would improve the miscibility of lignin with sulfur and simultaneously introduce olefin moieties capable of crosslinking with sulfur.

The principal method to prepare high sulfur-content materials (HSMs) is inverse vulcanization (Scheme 1A).[10–13] Inverse vulcanization employs sulfur as the majority component but is mechanistically identical to Goodyear's traditional vulcanization,[2] which employs <5 wt% of elemental sulfur. Inverse vulcanization involves thermal formation of [$^{\bullet}$S–S_n–S$^{\bullet}$] radicals at >159 °C, whereby subsequent addition of these sulfur-centered radicals to C–C π-bonds produces highly-crosslinked networks comprising stabilized sulfur catenates.[14–16] In the absence of side reactions, inverse vulcanization is 100% atom-economical. HSMs have been explored for a wide range of possible uses such as components of lithium-sulfur batteries,[17–21] thermal imaging lenses,[22] adhesives,[23] water

[a]Department of Chemistry, Clemson University, Clemson, South Carolina, 29634, USA. E-mail: rhett@clemson.edu

[b]Department of Materials Science and Engineering, Clemson University, Clemson, South Carolina, 29634, USA

† Electronic supplementary information (ESI) available: Proton NMR spectral data, FTIR spectra, TGA curves, DSC curves, DMA curves, and stress–strain plots. See DOI: https://doi.org/10.1039/d2ra07082k

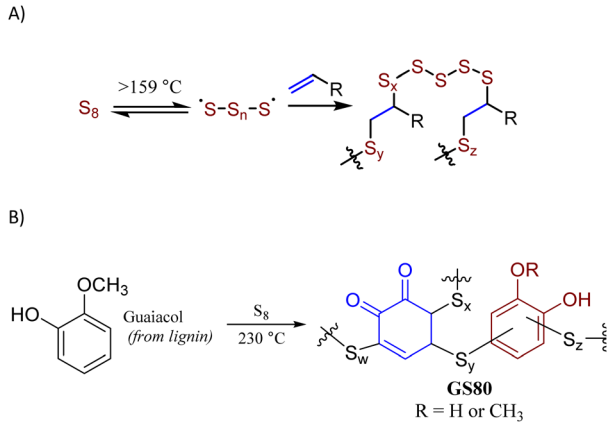

Scheme 1 Formation of HSMs by inverse vulcanization (A) or by reaction of sulfur with guaiacol thermal decomposition products (B).

purification media,[24–28] and fertilizers.[29–31] A wide range of innovative, lower-temperature processing and recycling techniques have also been explored.[29,32–36] Sustainability of HSMs has been further improved by using biologically-produced olefin comonomers, such as lignin derivatives,[5,6,8,9] cellulose derivatives,[37,38] starch,[39–42] raw lignocellulosic biomass,[43,44] fatty acids,[45–47] triglycerides,[48,49] terpenoids,[38,50] and amino acid derivatives.[51] Miscibility issues for hydrophilic olefin sources during the HSM-forming reaction has been observed in some of these studies and could be addressed by using extended reaction times, adding compatibilizing agents/catalysts, or mechanochemical synthesis.

Whereas inverse vulcanization temperatures are generally 160–180 °C, alternative higher-temperature (220–320 °C) conditions can allow HSM formation *via* the reaction of sulfur with aromatic moieties to yield S–C_{aryl} bonds, in addition to any S–C_{alkyl} bonds derived from olefinic moieties in the monomers. Aryl halides, for example, decompose above 220 °C in the presence of sulfur to give sulfur-reactive aryl radicals, affording HSMs *via* a process termed radical-induced aryl halide–sulfur polymerization (RASP).[9] Anisole derivatives likewise form HSMs when they undergo thermal decomposition in the presence of sulfur at 220–320 °C, whereupon several moieties undergo facile S–C bond-formation with sulfur or sulfur-centered radicals. This route has been used to prepare durable composite GS80 from guaiacol (Scheme 1B) as well as several HSMs from bisphenol A derivatives.[33,34,52,53] At sufficiently low crosslink densities, most HSMs produced by these processes can be recycled by simple melt-casting, owing to the thermal reversibility of S–S bond breakage/formation.[54–59]

Kraft (alkali) lignin like that used in the current work has a complex structure (Fig. 1)[60] comprising several types of structural subunits that undergoes partial thermal decomposition to form anisole derivatives like guaiacol at 230 °C. We hypothesized that the reaction conditions for the conversion of guaiacol to GS80 would likewise yield HSMs from oleic acid-esterified lignin comprising S–C_{aryl} and S–C_{alkyl} bonds. In contrast, reaction of esterified lignin with elemental sulfur at 180 °C would be limited to olefin crosslinking by inverse

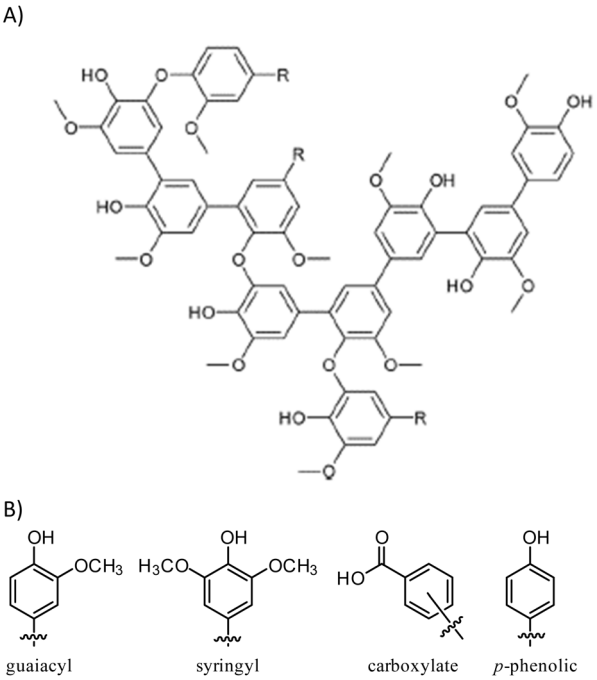

Fig. 1 (A) Generalized structure of lignin, and (B) classification of hydroxyl-bearing subunits that can be found in lignin. Part A is © Royal Society of Chemistry and reproduced from *Green Chem.*, 2017, **19**, 4104–4121 with permission.

vulcanization to give HSMs comprising primarily S–C_{alkyl} crosslinks. Herein we report the reaction of oleic acid-esterified lignin with elemental sulfur (80 or 90 wt%) at 180 °C and 230 °C to afford composites. The extent to which composite properties are influenced by monomer feed ratio and reaction temperature are discussed.

Results and discussion

The primary objectives of the current study were to improve lignin incorporation into HSMs and to elucidate the influence of reaction temperature on composite properties. Lignin incorporation into HSMs *via* inverse vulcanization is limited by the poor miscibility of hydrophilic lignin with hydrophobic sulfur. Oleic acid was selected as a derivatizing agent for lignin because it is readily obtained from various biological sources, provides a hydrophobic chain for miscibility with sulfur, provides additional olefin moieties for crosslinking, and undergoes facile esterification with lignin hydroxyl groups. The same lot of lignin used for previously reported HSMs was used in this study as well.[8] Lignin was esterified *via* acid-catalysed reaction with oleic acid (Scheme 2) in water at room temperature *via* a reported green chemical process.[61] Excess oleic acid was removed by recursive dialysis using a 14 kDa cut-off membrane to give EL (Scheme 2).

Total olefin content of esterified lignin (EL) was quantified by integration of the olefinic resonance at 5.3 ppm in the ^{1}H NMR spectrum to the aldehydic resonance at 10.3 ppm for the internal standard, 2,3,4,5,6-pentafluorobenzaldehyde (ESI

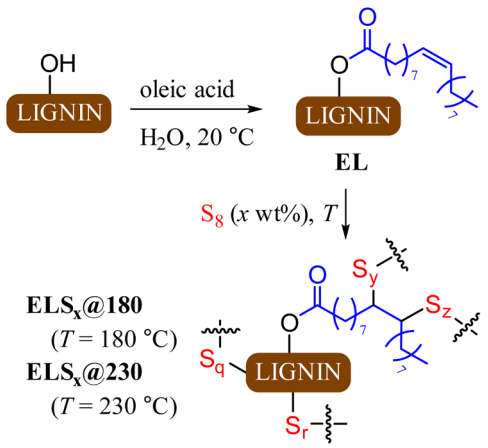

Scheme 2 Esterification of lignin to form EL followed by inverse vulcanization of EL to form composites ELS_x at 180 or 230 °C.

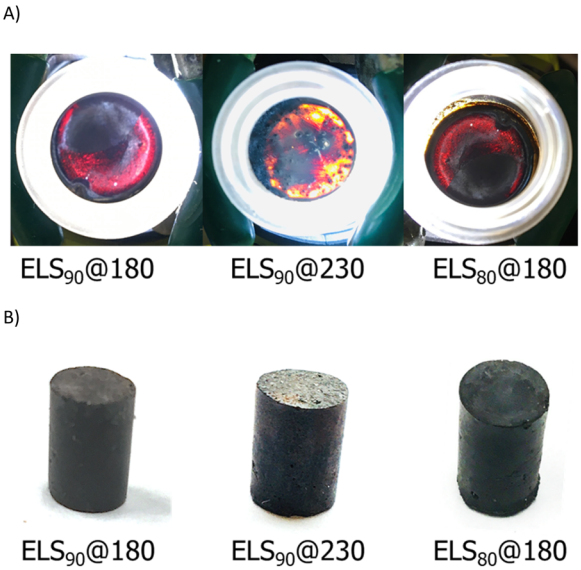

Fig. 2 Digital images of back-lit samples (A) and of compressive strength test cylinders (B) of ELS composites.

Fig. S1†). This analysis revealed the olefin content in EL to be 0.24 mmol g^{-1}. Quantification of lignin's total hydroxyl content and of the contribution of each class of hydroxyl-bearing subunit (aliphatic, guaiacyl, syringyl, *p*-phenolic or carboxylate, Fig. 1) was accomplished using ^{31}P NMR spectrometry of phosphitylated lignin following the reported method (ESI Fig. S2†).[62,63] Calculations from a comparison of total hydroxyl content for precursor lignin to that of EL reveal that 7.5% of available hydroxyl sites had been esterified in its conversion to EL. This is consistent with low percentage modification due to the highly crosslinked nature of lignin and consequent inaccessibility of some potential esterification sites.

Each reaction of EL with elemental sulfur was carried out in a sealed tube under an atmosphere of dry nitrogen at either 180 °C or 230 °C, affording composites ELS_x@180 and ELS_x@230, respectively (x = 80 or 90 wt% sulfur). The reaction mixtures for ELS_{80}@180, ELS_{90}@180, and ELS_{90}@230 remained homogenous for the duration of heating, confirming improved miscibility of sulfur and oleyl-modified EL. Effort to prepare ELS_{80}@230 led to separation of an intractable solid during reaction, so this reaction was not further pursued. The miscibility of EL and sulfur thus has an upper limit of between 10 and 20 wt% at 230 °C where greater crosslinking is expected. For materials resulting from the homogeneous reaction mixtures, elemental microanalysis confirmed that all lignin in the monomer feed was incorporated into the final composites. Scanning electron microscopy with elemental mapping by energy-dispersive X-ray analysis (SEM-EDX) further confirmed that the distribution of C and S in the solids was uniform (Fig. S3, ESI†). This is in sharp contrast to reactions of allylated lignin with sulfur, wherein lignin incorporation never exceeded 5 wt%, even if the monomer feed contained 20 wt% lignin derivative.

Upon cooling to room temperature, ELS_{90}@180, ELS_{80}@180, and ELS_{90}@230 were isolated as readily-remeltable, deep red- to orange-colored solids (Fig. 2). The color of sulfur catenates range from pale yellow for *cyclo*-S_8 to deep red for polymeric sulfur catenates.[14,64] The deep red color observed in ELS_x@180 is diagnostic for the presence of polymeric sulfur catenates in the crosslinked network. The orange color of ELS_{90}@230 is consistent with shorter average sulfur catenate lengths that are expected from increased crosslinking at 230 *versus* 180 °C.

Thermogravimetric analysis (TGA) revealed a mass loss event at just above 230 °C (Table 1 and ESI Fig. S4†), similar to that observed in the sublimation of *cyclo*-S_8. In ELS, this mass loss can be attributed to sublimation of *cyclo*-S_8 entrapped within ELS but not covalently bound to the crosslinked network. Although this mass loss is near the reaction temperature, no mass loss is observed during the reaction because it is performed in a sealed vessel, and any sublimed sulfur depositing on the interior sides of the vessel will melt and return to the reaction mixture. The derivative TGA curve for ELS_{90}@230 (Fig. S2, ESI†) exhibited a decomposition event slightly above 300 °C, attributable to decomposition of the highly-crosslinked aromatic network.[60] Similar thermogravimetric features are displayed by the decomposition of other HSMs comprising highly aromatic organic monomers.[7,8,33,34,53]

Table 1 Physical and thermal properties of lignin biomass–sulfur materials

Materials	T_d[a]/°C	T_g[a]/°C	T_{cc}[b]/°C	T_m[c]/°C
S_8	228	NA	NA	120
ELS_{90}@180	230	−37	−9 to −13 32 to 44	117
ELS_{90}@230	234	−37	−18 to 7 32 to 44	117
ELS_{80}@180	231	−37	−10 to 10 37 to 48	117

[a] Decomposition temperature, here defined as the temperature at which 5% mass loss was observed. [b] Cold crystallization temperature. [c] Melting temperature.

Thermograms obtained by differential scanning calorimetry (DSC, Fig. S5, ESI†) of ELS composites each revealed features typical of other lignin-incorporating HSMs. Glass transitions at −37 °C are diagnostic for polysulfur catenates and cold crystallization peaks are frequently observed for HSMs as a result of morphological changes in these partially organized polymeric sulfur domains. Endothermic peaks at ~120 °C are attributable to melting of *cyclo*-S_8 physically trapped in the material but not covalently incorporated into the crosslinked network. The entrapped, unreacted *cyclo*-S_8 was extracted from each composite using carbon disulfide (CS_2). Elemental microanalysis confirmed that the CS_2-soluble fraction contained only elemental sulfur for ELS_{90}@180 and ELS_{80}@180, thus allowing its quantification. Increased crosslinking caused by higher lignin content predictably yielded more covalently-incorporated sulfur: 16% of added sulfur was covalently trapped in ELS_{90}@180, while 23% was covalently trapped in ELS_{80}@180. These values are typical for similarly-crosslinked HSMs comprising 80–90 wt% sulfur. The partial decomposition of lignin backbone at 230 °C led to some low molecular organic fragments in the soluble fraction of ELS_{90}@230, so free *cyclo*-S_8 alone could not be quantified by this method. Because the amount of covalently-linked sulfur was quantifiable for ELS_{90}@180 and ELS_{80}@180, it was possible to calculate the sulfur rank (average number of sulfur atoms per oligo-/polysulfur crosslink) to be 48 in ELS_{90}@180 and 12 in ELS_{80}@180. Shorter crosslink chains are consistent with higher crosslinking for higher lignin content. These sulfur ranks are also consistent with those of other HSMs comprising 80–90 wt% sulfur and similar olefin content.[8,65]

Microstructures in ELS composites were elucidated *via* partial depolymerization with $AlBr_3$ followed by GC-MS analysis of the fragments following a procedure reported previously.[9] No fragments were observed that would be expected of species comprising S–C_{aryl} bonds in the ELS composites prepared at 180 °C, which indicated that crosslinking occurred primarily *via* inverse vulcanization of the olefinic moieties. In contrast, several microstructural subunits having S–C_{aryl} bonds were observed in GC-MS analysis of soluble depolymerization fractions of ELS_{90}@230 (Fig. 3, mass spectra provided in ESI Fig. S6†). These functionalities are the same structural subunits observed in the analogous analysis of GS80 and of other HSMs prepared by the reaction of anisole derivatives with sulfur above 230 °C.

For ELS composites to supplant less sustainable construction materials, they must meet application-specific mechanical strength requirements. Ordinary Portland cement (OPC), for example, must have flexural strength > 3 MPa and compressive strength ≥ 17 MPa (ACI specification 332.1R-06) to be used in residential dwelling foundations (representative stress–strain and plots are provided in ESI Fig. S7–S12†). Mechanical strength characteristics of ELS composites are displayed graphically in Fig. 4. For lignin–sulfur composites synthesized by inverse vulcanization, the highest reported flexural strength is 2.1 MPa for LS_{80}, comprising 5% allylated lignin and 95 wt% sulfur.[8] The flexural strength values for ELS_{90}@180 (3.3 MPa) and ELS_{80}@180 (2.7 MPa) were comparable, and somewhat higher than that of LS_{80}, reflecting the greater extent of lignin incorporation in the ELS composites. The highest flexural strength previously reported for a lignin–sulfur composite is 3.6 MPa for CLS_{80}, a composite prepared *via* RASP of 20 wt% chlorolignin with 80 wt% elemental sulfur at 230 °C.[9] With a flexural strength of 3.9 MPa, ELS_{90}@230 exceeds the previous mark due to crosslinking of olefins in ELS whereas only crosslinking through S–C_{aryl} bonds is possible in CLS_{80}. An even higher flexural strength (5.6 MPa) has been reported for

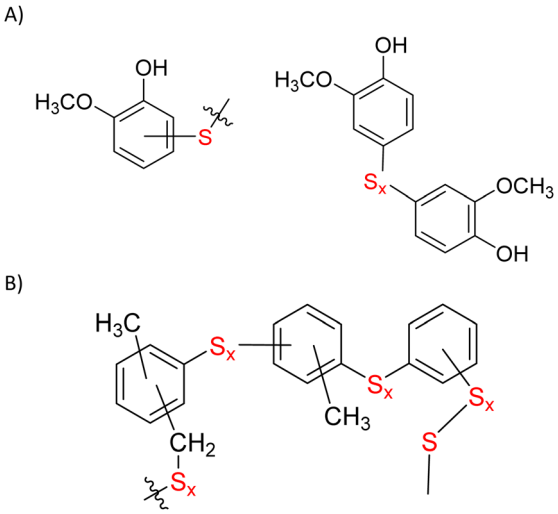

Fig. 3 Some microstructural subunits derived directly from guaiacyl units (A) or from thermal methyl migration decomposition products of guaiacyl/syringyl units (B) deduced from fractionation studies of both ELS_{90}@230 and GS80 confirm the formation of S–C_{aryl} bonds. None of these subunits was observed in analysis of ELS_x@180 materials. Mass spectra corresponding to these structural subunits are provided in ESI Fig. S6.†

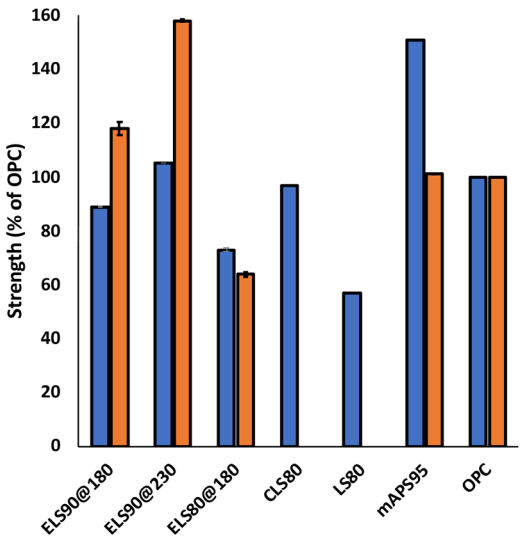

Fig. 4 Comparison of compressive (orange bars) and flexural (blue bars) strengths of lignin- and lignin/cellulose-containing HSMs normalized to those of an ordinary Portland cement (OPC) for residential building (flexural strength = 3.5 MPa, compressive strength = 17 MPa).

composite $mAPS_{95}$,[43,66] a composite prepared by inverse vulcanization of a mixture of allyl lignin (2 wt%), allyl cellulose (3 wt%) and 95 wt% sulfur. In this material, the high flexural strength could also be attributed to increased crosslink density from lignin–cellulose crosslinks, in addition to sulfur–olefin crosslinks. Overall, the flexural strength characteristics of the ELS composites are competitive with both load-bearing materials, such as OPC, and nonstructural components, such as Azdel SuperLite® (glass fibre–polypropylene used in automotive door panels).[67]

Compressive strengths have not been reported for CLS_{80} or LS_{80}, but the compressive strength of $mAPS_{95}$ (17 MPa) is competitive with OPC and compressive strengths of up to 36 MPa have been reported for other HSMs comprising highly-allylated raw biomass and sulfur.[43,66] The compressive strengths of ELS composites follow flexural strength trends, with a low of 10.9 MPa for ELS_{80}@180, followed by ELS_{90}@180 (20.1 MPa) and a high of 26.8 MPa for ELS_{90}@230. The lower flexural and compressive strength of ELS_{80}@180 as compared to that of less-crosslinked ELS_{90}@180 may seem counterintuitive, but prior work has demonstrated that there is an upper limit to mechanical strength improvements as a function of added organic material for some monomers.[52] A higher strength may therefore be attainable when a lower wt% of organic material for which there are more crosslinkable sites per unit mass. This hypothesis is supported by the increase in strength observed in ELS_{90}@230.

Conclusions

Herein we report a method to modify lignin with oleic acid to increase the number of reactive olefin sites and miscibility with sulfur. Improved miscibility allowed up to 20 wt% lignin incorporation into remeltable HSMs. Crosslink density has a significant impact on properties of HSMs. In this study, crosslink density was tuned by changing the proportion of monomer feed lignin (10 or 20 wt%) or by the selection of reaction temperature (180 °C or 230 °C). At 180 °C inverse vulcanization occurs, leading to S–C_{alkyl} bond formation. At 230 °C both inverse vulcanization and reaction of sulfur with lignin's thermal decomposition products occur, facilitating both S–C_{alkyl} and S–C_{aryl} bond formation. Composite flexural and compressive strengths were highest when 90 wt% lignin was reacted with sulfur at 230 °C to give ELS_{90}@230. Composite ELS_{90}@230 exhibits flexural (3.9 MPa) and compressive (26.8 MPa) strengths exceeding those of some commercial fibre-reinforced polymer composites and traditional mineral cements used in residential building. These composites thus represent a potential lignin valorisation option that also replaces commercial products whose manufacture produces >8% of anthropogenic CO_2 emissions.[68]

Experimental

General considerations

All NMR spectra were recorded on a Bruker Avance spectrometer operating at 300 MHz for proton and 121.5 MH for phosphorus. Thermogravimetric analysis (TGA) data were recorded on a TA SDT Q600 instrument over the range 25 to 800 °C, with a heating rate of 5 °C min^{-1} under a flow of N_2 (20 mL min^{-1}). Differential scanning calorimetry (DSC) data were acquired using a Mettler Toledo DSC 3 STARe System over the range of −60 to 140 °C, with a heating rate of 10 °C min^{-1} under a flow of N_2 (50 mL min^{-1}). Each DSC measurement was carried out over three heat–cool cycles, and data are reported for the third cycle. Fourier transform infrared spectra were obtained using a Shimadzu IR Affinity-1S instrument operating over the range of 400–4000 cm^{-1} at ambient temperature using an ATR attachment.

Flexural strength analysis was performed using a Mettler Toledo DMA 1 STARe System in single cantilever mode. The samples were cast from silicone resin molds (Smooth-On Oomoo® 30 tin-cure). The sample dimensions were 1.5 × 10 × 23 mm. Flexural analysis was performed in duplicate and results were averaged. The clamping force was 1 cN m Compressional analysis was performed on a Mark-10 ES30 test stand equipped with a M3-200 force gauge (1 kN maximum force with ±1 N resolution). Compression cylinders were cast from silicone resin moulds (Smooth-On Oomoo® 30 tin-cure) with diameters of ∼6 mm and heights of ∼8 mm. Samples were manually sanded to ensure uniform dimensions. Compressional analysis was performed in triplicate and results were averaged.

The GC-MS analysis was carried out on a Shimadzu QP2010SE system with an auto injector (AOC-20i), equipped with mass selective detector, having interface temperature of 250 °C, a solvent cut time of 3.00 min, threshold of 70 eV and mass range of 45 to 900 *m*/*z*. Compounds were separated using a SH-Rxi-5 MS capillary column (Restek Company, Bellefonte, USA: crossbond 5% diphenyl/95% dimethyl polysiloxane) having dimensions 30 m (length) × 0.25 mm (diameter) × 0.25 μm (film thickness). The temperature of the injector was initialized to 250 °C. The temperature was programmed from 40 °C to 320 °C at a ramp rate of 10 °C min^{-1}.

Materials and methods

Alkali lignin was purchased from Sigma-Aldrich. Sulfur powder (99.5%) and oleic acid (99%) were purchased from Alfa Aesar. Carbon disulfide was purchased from Bean Town Chemical. Esterification of lignin with oleic acid to prepare EL followed the literature report.[61]

Synthesis of EL

EL was synthesized following the literature report[61] and degree of substitution assessed by integration of ^{1}H NMR signals for oleoyl-derived alkene signals *versus* those of 2,3,4,5,6-pentafluorobenzaldehyde internal standard. ^{1}H NMR (300 MHz, DMSO-d_6, δ). Integrations are *versus* those of the resonance for the internal standard peak at 10.1 ppm, which was normalized to an integration of 1.00: 0.65–0.95 (br. m, 0.65H), 1.0–1.4 (br. m, 3.16H), 1.4–1.7 (br. m, 0.60H), 1.9–2.1 (br. m, 0.65H), 2.9–4.4 (br. m, 10.4H), 5.1–5.6 (br. m, 0.23H), 6.2–7.3 (br. m, 4.09H), 7.3–7.6 (br. m, 0.29H).

General synthesis of ELS composites

CAUTION: Heating elemental sulfur with organics can result in the formation of H_2S gas. H_2S is toxic, foul smelling, and corrosive. Although we did not observe any mass loss attributable to gas generation, temperature must be carefully controlled to prevent thermal spikes, which contribute to the potential for H_2S evolution. Rapid stirring, shortened heating times, and very slow addition of reagents can help prevent unforeseen temperature spikes.

The required amounts of elemental sulfur and esterified lignin were weighed directly into a pressure tube under an inert N_2(g) environment. Two oil baths were set up at 180 and 230 °C and two samples for each temperature were prepared using 10 or 20 wt% EL with elemental sulfur. Heating was continued for 24 h with continuous stirring with a magnetic stir bar. No mass loss was observed for any of the reaction tubes, so the solids were isolated in quantitative yield. For ELS_{90}@230 a small amount of elemental sulfur sublimes and 1% of mass is lost due to this. For the reactions carried out at 180 °C recovery is quantitative.

Elemental microanalysis for ELS_{90}@180. Elemental analysis calcd: C 7.4%, H 0.6%, S 90%; found: C 7.9%, H 0.5%, S 90.2%. The CS_2-soluble fraction is 99.2 ± 0.4% sulfur.

Elemental microanalysis for ELS_{80}@180. Elemental analysis calcd: C 14.8%, H 1.2%, S 80%; found: C 14.5%, H 1.1%, S 78.2%. The CS_2-soluble fraction is 99.4 ± 0.4% sulfur.

Elemental microanalysis for ELS_{90}@230. Elemental analysis calcd: C 7.4%, H 0.6%, S 90%; found: C 8.4%, H 0.5%, S 89.4% (~1% of the sulfur is lost through sublimation). The CS_2-soluble fraction is 98.7 ± 0.4% sulfur.

Author contributions

MKL, CPM and MSK: data curation, formal analysis, investigation, validation. RCS: writing – original draft, conceptualization, funding acquisition, methodology, resources, supervision. AGT: writing – review and editing, resources, supervision.

Conflicts of interest

There are no conflicts to declare.

Acknowledgements

This research is funded by the National Science Foundation grant number CHE-2203669 to RCS.

Notes and references

1 J. Lim, J. Pyun and K. Char, *Angew. Chem., Int. Ed.*, 2015, **54**, 3249–3258.
2 C. Goodyear, Improvement in India-Rubber Fabrics, USA, *US Pat.*, Patent Number: US3633A, 1844.
3 J. Zakzeski, P. C. A. Bruijnincx, A. L. Jongerius and B. M. Weckhuysen, *Chem. Rev.*, 2010, **110**, 3552–3599.
4 J. Stevens and D. J. Gardner, *Wood Fiber Sci.*, 2010, **42**, 439–443.
5 M. S. Karunarathna and R. C. Smith, *Sustainability*, 2020, **12**, 734–748.
6 M. S. Karunarathna, M. K. Lauer and R. C. Smith, *J. Mater. Chem. A*, 2020, **8**, 20318–20322.
7 M. S. Karunarathna, M. K. Lauer, A. G. Tennyson and R. C. Smith, *Polym. Chem.*, 2020, **11**, 1621–1628.
8 M. S. Karunarathna, M. K. Lauer, T. Thiounn, R. C. Smith and A. G. Tennyson, *J. Mater. Chem. A*, 2019, **7**, 15683–15690.
9 M. S. Karunarathna, A. G. Tennyson and R. C. Smith, *J. Mater. Chem. A*, 2020, **8**, 548–553.
10 W. J. Chung, J. J. Griebel, E. T. Kim, H. Yoon, A. G. Simmonds, H. J. Ji, P. T. Dirlam, R. S. Glass, J. J. Wie, N. A. Nguyen, B. W. Guralnick, J. Park, A. Somogyi, P. Theato, M. E. Mackay, Y.-E. Sung, K. Char and J. Pyun, *Nat. Chem.*, 2013, **5**, 518–524.
11 M. Chalker Justin, J. H. Worthington Max, A. Lundquist Nicholas and J. Esdaile Louisa, *Top. Curr. Chem.*, 2019, **377**, 16.
12 D. A. Boyd, *Angew. Chem., Int. Ed. Engl.*, 2016, **55**, 15486–15502.
13 M. J. H. Worthington, R. L. Kucera and J. M. Chalker, *Green Chem.*, 2017, **19**, 2748–2761.
14 B. Meyer, *Chem. Rev.*, 1964, **64**, 429–451.
15 *Elemental Sulfur; Chemistry and Physics*, B. Meyer, 1965.
16 B. Meyer, *Inorg. Sulphur Chem.*, 1968, 241–258.
17 Z. Chen, J. Droste, G. Zhai, J. Zhu, J. Yang, M. R. Hansen and X. Zhuang, *Chem. Commun.*, 2019, **55**, 9047–9050.
18 F. Zhao, Y. Li and W. Feng, *Small Methods*, 2018, **2**, 1–34.
19 D. T. Nguyen, A. Hoefling, M. Yee, G. T. H. Nguyen, P. Theato, Y. J. Lee and S.-W. Song, *ChemSusChem*, 2019, **12**, 480–486.
20 H. Mutlu, P. Theato, B. Ceper Ezgi, M. Ozmen Mehmet, X. Li, J. Yang, W. Dong, P. Theato and J. Yang, *Macromol. Rapid Commun.*, 2019, **40**, e1800650.
21 C. V. Lopez, C. P. Maladeniya and R. C. Smith, *Electrochem*, 2020, **1**, 226–259.
22 J. J. Griebel, S. Namnabat, E. T. Kim, R. Himmelhuber, D. H. Moronta, W. J. Chung, A. G. Simmonds, K.-J. Kim, J. van der Laan, N. A. Nguyen, E. L. Dereniak, M. E. MacKay, K. Char, R. S. Glass, R. A. Norwood and J. Pyun, *Adv. Mater.*, 2014, **26**, 3014–3018.
23 A. E. Davis, K. B. Sayer and C. L. Jenkins, *Polym. Chem.*, 2022, **13**, 4634–4640.
24 H.-K. Lin, Y.-S. Lai and Y.-L. Liu, *ACS Sustainable Chem. Eng.*, 2019, **7**, 4515–4522.
25 A. M. Abraham, S. V. Kumar and S. M. Alhassan, *Chem. Eng. J.*, 2018, **332**, 1–7.
26 D. J. Parker, H. A. Jones, S. Petcher, L. Cervini, J. M. Griffin, R. Akhtar and T. Hasell, *J. Mater. Chem. A*, 2017, **5**, 11682–11692.
27 S. Akay, B. Kayan, D. Kalderis, M. Arslan, Y. Yagci and B. Kiskan, *J. Appl. Polym. Sci.*, 2017, **134**, 45306.
28 T. Hasell, D. J. Parker, H. A. Jones, T. McAllister and S. M. Howdle, *Chem. Commun.*, 2016, **52**, 5383–5386.

29 N. A. Lundquist, A. D. Tikoalu, M. J. H. Worthington, R. Shapter, S. J. Tonkin, F. Stojcevski, M. Mann, C. T. Gibson, J. R. Gascooke, A. Karton, L. C. Henderson, L. J. Esdaile and J. M. Chalker, *Chem.–Eur. J.*, 2020, **26**, 10035–10044.
30 S. F. Valle, A. S. Giroto, R. Klaic, G. G. F. Guimaraes and C. Ribeiro, *Polym. Degrad. Stab.*, 2019, **162**, 102–105.
31 M. Mann, J. E. Kruger, F. Andari, J. McErlean, J. R. Gascooke, J. A. Smith, M. J. H. Worthington, C. C. C. McKinley, J. A. Campbell, D. A. Lewis, T. Hasell, M. V. Perkins and J. M. Chalker, *Org. Biomol. Chem.*, 2019, **17**, 1929–1936.
32 P. Yan, W. Zhao, F. McBride, D. Cai, J. Dale, V. Hanna and T. Hasell, *Nat. Commun.*, 2022, **13**, 4824.
33 T. Thiounn and R. C. Smith, *J. Polym. Sci.*, 2020, **58**, 1347–1364.
34 T. Thiounn, M. S. Karunarathna, L. M. Slann, M. K. Lauer and R. C. Smith, *J. Polym. Sci.*, 2020, **58**, 2943–2950.
35 S. J. Tonkin, C. T. Gibson, J. A. Campbell, D. A. Lewis, A. Karton, T. Hasell and J. M. Chalker, *Chem. Sci.*, 2020, **11**, 5537–5546.
36 K. Orme, A. H. Fistrovich and C. L. Jenkins, *Macromolecules*, 2020, **53**, 9353–9361.
37 M. K. Lauer, T. A. Estrada-Mendoza, C. D. McMillen, G. Chumanov, A. G. Tennyson and R. C. Smith, *Adv. Sustainable Syst.*, 2019, **3**, 1900062.
38 M. K. Lauer, A. G. Tennyson and R. C. Smith, *ACS Appl. Polym. Mater.*, 2020, **2**, 3761–3765.
39 M. K. Lauer and R. C. Smith, *Compr. Rev. Food Sci. Food Saf.*, 2020, 1–53, DOI: **10.1111/1541-4337.12627**.
40 M. K. Lauer, A. G. Tennyson and R. C. Smith, *Mater. Adv.*, 2021, **2**, 2391–2397.
41 M. K. Lauer, A. G. Tennyson and R. C. Smith, *Mater. Adv.*, 2022, **3**, 4186–4193.
42 M. K. Lauer, Z. E. Sanders, A. D. Smith and R. C. Smith, *Mater. Adv.*, 2021, **2**, 7413–7422.
43 M. K. Lauer, M. S. Karunarathna, A. G. Tennyson and R. C. Smith, *Mater. Adv.*, 2020, **1**, 590–594.
44 M. K. Lauer, M. S. Karunarathna, G. Tennyson Andrew and R. C. Smith, *Mater. Adv.*, 2020, **1**, 2271–2278.
45 A. D. Smith, C. D. McMillin, R. C. Smith and A. G. Tennyson, *J. Polym. Sci.*, 2020, **58**, 438–445.
46 A. D. Smith, R. C. Smith and A. G. Tennyson, *Sustainable Chem. Pharm.*, 2020, **16**, 100249.
47 A. D. Smith, R. C. Smith and A. G. Tennyson, *Sustainable Chem.*, 2020, **1**, 209–237.
48 C. V. Lopez, M. S. Karunarathna, M. K. Lauer, C. P. Maladeniya, T. Thiounn, E. D. Ackley and R. C. Smith, *J. Polym. Sci.*, 2020, **58**, 2259–2266.
49 C. V. Lopez, A. D. Smith and R. C. Smith, *RSC Adv.*, 2022, **12**, 1535–1542.
50 C. P. Maladeniya, M. S. Karunarathna, M. K. Lauer, C. V. Lopez, T. Thiounn and R. C. Smith, *Mater. Adv.*, 2020, **1**, 1665–1674.
51 T. Thiounn, A. G. Tennyson and R. C. Smith, *RSC Adv.*, 2019, **9**, 31460–31465.
52 T. Thiounn, M. K. Lauer, M. S. Bedford, R. C. Smith and A. G. Tennyson, *RSC Adv.*, 2018, **8**, 39074–39082.
53 T. Thiounn, M. K. Lauer, M. S. Karunarathna, A. G. Tennyson and R. C. Smith, *Sustainable Chem.*, 2020, **1**, 183–197.
54 A. D. Smith, T. Thiounn, E. W. Lyles, E. K. Kibler, R. C. Smith and A. G. Tennyson, *J. Polym. Sci., Part A: Polym. Chem.*, 2019, **57**, 1704–1710.
55 B. T. Michal, C. A. Jaye, E. J. Spencer and S. J. Rowan, *ACS Macro Lett.*, 2013, **2**, 694–699.
56 J. J. Griebel, N. A. Nguyen, S. Namnabat, L. E. Anderson, R. S. Glass, R. A. Norwood, M. E. MacKay, K. Char and J. Pyun, *ACS Macro Lett.*, 2015, **4**, 862–866.
57 A. J. R. Amaral and G. Pasparakis, *Polym. Chem.*, 2017, **8**, 6464–6484.
58 M. Arslan, B. Kiskan and Y. Yagci, *Sci. Rep.*, 2017, **7**, 1–11.
59 A. Takahashi, R. Goseki, K. Ito and H. Otsuka, *ACS Macro Lett.*, 2017, **6**, 1280–1284.
60 C. Crestini, H. Lange, M. Sette and D. S. Argyropoulos, *Green Chem.*, 2017, **19**, 4104–4121.
61 L. An, C. Si, G. Wang, C. S. Choi, Y. H. Yu, J. H. Bae, S. M. Lee and Y. S. Kim, *BioResources*, 2020, **15**, 89–104.
62 D. S. Argyropoulos, *J. Wood Chem. Technol.*, 1994, **14**, 45–63.
63 D. S. Argyropoulos, H. I. Bolker, C. Heitner and Y. Archipov, *J. Wood Chem. Technol.*, 1993, **13**, 187–212.
64 C. B. Meyer, T. Stroyer-Hansen, D. Jensen and T. V. Oommen, *J. Am. Chem. Soc.*, 1971, **93**, 1034–1035.
65 M. K. Lauer, T. A. Estrada-Mendoza, C. D. McMillen, G. Chumanov, A. G. Tennyson and R. C. Smith, *Adv. Sustainable Syst.*, 2019, **3**, 1900062.
66 M. K. Lauer, M. S. Karunarathna, A. G. Tennyson and R. C. Smith, *Mater. Adv.*, 2020, **1**, 2271–2278.
67 Technical data sheet "Azdel SuperLite® SL550600-100" Supplied by Azdel April 30, 2020.
68 K. L. Scrivener, V. M. John and E. M. Gartner, *Cem. Concr. Res.*, 2018, **114**, 2–26.